The evolution of the ordered states of single-crystal URu_2Si_2 under pressure

2008 J. Phys.: Condens. Matter 20 095225

(http://iopscience.iop.org/0953-8984/20/9/095225)

J. Phys.: Condens. Matter **20** (2008) 095225 (9pp) doi:10.1088/0953-8984/20/9/095225

The evolution of the ordered states of single-crystal URu_2Si_2 under pressure

J R Jeffries[1], N P Butch, B T Yukich and M B Maple

Department of Physics and Institute for Pure and Applied Physical Sciences, University of California, San Diego, La Jolla, CA 92093, USA

E-mail: jeffries4@llnl.gov

Received 3 December 2007
Published 15 February 2008
Online at stacks.iop.org/JPhysCM/20/095225

Abstract

The 'hidden order' (HO) and superconducting (SC) states of URu_2Si_2 have been investigated via electrical resistivity measurements as a function of pressure P up to nearly 30 kbar and magnetic field $H \leqslant 9$ T. The field and pressure dependences of the SC state were examined for two crystals with H aligned parallel to c and a, with the latter orientation revealing an enhanced critical field. No discontinuities in either the field or pressure dependence of the SC state were found. The evolution of the HO state showed a distinct kink in the pressure dependence at $P_c = 15$ kbar, coincident with the destruction of superconductivity. The behavior of the two ordered phases was analyzed via a model describing the competition for Fermi surface fraction, where a portion of the Fermi surface becomes completely gapped near P_c. The evolution of the magnitude of the scattering at the HO transition is compared with the Fermi surface fraction gapped by the HO state, and the phenomenology of a spin density wave-like ground state is discussed as it pertains to the data presented.

(Some figures in this article are in colour only in the electronic version)

1. Introduction

The heavy fermion compound URu_2Si_2 has captivated both experimentalists and theorists since its discovery over 20 years ago [1–3]. The broad interest in this material has been primarily due to the presence of pronounced yet poorly understood phenomena, the most egregious of which being the 'hidden order' (HO) state—so called as the order parameter has yet to be satisfactorily identified—occurring below $T_0 = 17.5$ K at ambient pressure. In addition to the HO transition, an unconventional superconducting state develops below $T_c \approx 1.5$ K, exemplifying the complexities inherent to uranium compounds with strongly correlated electron behavior.

Associated with the HO transition is a large BCS-like jump in the specific heat and a pronounced spin-density-wave-like anomaly in the electrical resistivity. The magnitude of the specific heat jump corresponds to a significant release of entropy $\Delta S \approx 0.2R \ln 2$. However, the low-temperature magnetic moment determined from neutron scattering measurements was found to be $\sim 0.03\mu_B$/U ion [4], a value much too small to account for the entropy released in the transition. The resolution of this small moment associated with the HO transition seen in virtually all macroscopic measurements has been the driving force behind much experimental and theoretical work, including numerous models to explain the ordering such as incommensurate orbital antiferromagnetism [5], crystalline-electric-field-induced multipolar order [6–8], concomitant local and itinerant magnetism [9], triple-spin correlators [10], conventional and unconventional spin density waves [11, 12], spin nematics [13], and helicity order [14]. In addition to theoretical work, experimentalists have performed many measurements to both characterize URu_2Si_2 and constrain theoretical models.

The compound URu_2Si_2 crystallizes in the $ThCr_2Si_2$ tetragonal crystal structure with lattice constants $a = 4.14$ Å and $c = 9.56$ Å. Electrical resistivity and magnetization measurements reveal a broad maximum near 80 K followed by a rapid reduction in electrical resistivity associated with the formation of a heavy Fermi liquid ground state. The HO transition develops out of this Fermi liquid condensate and, as seen in electrical resistivity, is remarkably reminiscent of the archetypal spin density wave (SDW) transition seen in Cr [15]. Below the HO transition, the electrical resistivity is

[1] Present address: Lawrence Livermore National Laboratory, Livermore, CA, 94550, USA.

well-described by a formula combining a Fermi liquid term with a gapped magnon scattering term [16, 17]. The signature of the HO transition in specific heat is a large jump at T_0 followed by an exponential decrease in the specific heat with decreasing temperature, suggestive of a BCS-like transition opening a partial gap in the Fermi surface. Far-infrared optical conductivity, high-field magnetization, and thermal conductivity studies suggest that a charge or spin gap opens at the HO transition temperature [18–21], supporting speculation that the HO transition is associated with a charge density wave or spin density wave [3]. Still, these measurements have been unable to account for the presence of a small antiferromagnetic (AFM) moment in conjunction with the magnitude of the observed transitions.

High-pressure neutron scattering measurements have served to further enrich the phase diagram of URu_2Si_2 by revealing a significant increase in the size of the staggered moment for pressures in excess of $P_c \approx 15$ kbar [22]. Furthermore, high pressure electrical resistivity measurements have shown that the HO transition temperature T_0 undergoes a change in slope near P_c and that superconductivity is suppressed at a pressure slightly below P_c [16, 23]. The nature of this transition into the large moment antiferromagnetic (LMAFM) state at high pressure is still under considerable debate. Data obtained from μSR [24] and NMR [25, 26] measurements under pressure suggest that the small moment AFM state observed at zero pressure is merely a small, inhomogeneous volume fraction of the high-pressure LMAFM state phase segregated from the HO state. In this scenario, applied pressure serves to increase the volume fraction of the LMAFM phase while reducing that of the HO state. Another proposed phenomenological model is one in which two coupled order parameters, one being the magnetization of the LMAFM phase and one being the order parameter of the HO state, simultaneously transform to non-zero values below the transition temperature T_0 [27]. For the case of linearly coupled order parameters, the symmetries under which they transform must be identical, yielding a phase diagram with a first-order transition between a HO-dominated region and a LMAFM-dominated region. Other order parameter couplings yield first-order or second-order transitions between purely HO and LMAFM states. Recent experimental evidence from neutron scattering and thermal expansion under pressure appears to exhibit a sharp transition in the vicinity of 5–8 kbar, although the nature and order of this transition are unclear [28–30].

The superconducting state of URu_2Si_2 has been little explored, and its relation to the HO state or the LMAFM state could provide clues to the nature of the HO phase. The superconducting state has been shown to be anisotropic in its field and pressure dependence with respect to crystallographic axes [31–33]. Initial neutron scattering experiments revealed that the small moment persisted into the superconducting state, suggesting a coexistence of magnetism and superconductivity [4, 34]. Furthermore, it was suggested that the HO state and the superconducting state each gapped a portion of the Fermi surface, and that, with applied pressure, this competition for Fermi surface resulted in the suppression of T_c that accompanied the increase in T_0 [3]. In this paper, we report recent experimental investigations of the HO and superconducting states of single crystal samples of URu_2Si_2 as a function of both hydrostatic pressure and magnetic field.

2. Experimental details

Stoichiometric amounts of the constituent materials U, Ru, and Si were combined in a conventional single-arc furnace to form a boule of polycrystalline URu_2Si_2. Using the polycrystalline boule, single crystal samples of URu_2Si_2 were synthesized utilizing a tri-arc furnace equipped with a Czochralski crystal puller. Samples were annealed with a Zr getter at 900 °C for 7 days under 150 Torr of argon. After annealing, samples were aligned using the Laue method and spark cut into shapes suitable for electrical resistivity measurements within the pressure cells used.

High-temperature measurements ($T \geqslant 1$ K) as a function of temperature and pressure were performed in a pumped ^{4}He cryostat using a hydrostatic piston-cylinder cell. Low-temperature measurements (100 mK $\leqslant T \leqslant$ 2 K) as a function of temperature and pressure were performed in an Oxford Kelvinox MX-100 ^{3}He–^{4}He dilution refrigerator using a hydrostatic piston–cylinder cell. The pressure in the low-temperature experiments was determined from the HO transition temperature, calibrated from the high-temperature experiments that used the pressure-dependent superconducting critical temperature of lead to determine the pressure [35].

Initial high-temperature measurements performed using Fluorinert FC75 as the pressure-transmitting medium resulted in hysteretic behavior in the hidden order transition temperature with respect to increasing and decreasing pressure for pressures above approximately 14 kbar, near the room temperature hydrostatic limit of Fluorinert FC75 [36, 37]. As the ordered states of URu_2Si_2 have been shown to be sensitive to the crystalline axis along which pressure is applied [32, 33] and initial measurements showed hysteresis, a 1:1 mixture of n-pentane:isoamyl alcohol, which remains liquid at room temperature to pressures in excess of 30 kbar [38], was chosen as a pressure-transmitting medium for both high-temperature and low-temperature experiments to avoid inhomogeneous strains caused by non-hydrostatic conditions. Subsequent measurements performed using the n-pentane:isoamyl alcohol pressure-transmitting medium revealed no hysteresis upon depressurizing the cell. Electrical resistivity measurements were performed using a Linear Research LR-700 ac resistance bridge with excitation currents below 100 μA.

3. Results

3.1. Hidden order state

In an effort to investigate the evolution of the HO transition with applied pressure, pressure-dependent electrical resistivity measurements above 1 K have been performed on a sample of URu_2Si_2 with an ambient pressure residual resistivity ratio RRR = 7.2, where RRR is defined as the room temperature value of the electrical resistivity divided by

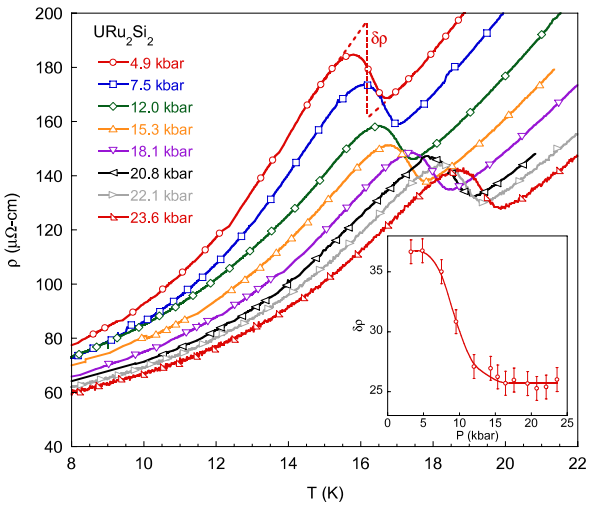

Figure 1. High-temperature $\rho(T)$ versus T of URu_2Si_2 for various pressures showing the progression of the hidden order transition. The dashed lines near the transition at $P = 4.9$ kbar are examples of extrapolations above and below T_0 used to quantify the height of the resistive anomaly associated with the HO transition $\delta\rho$. Inset: $\delta\rho$ as a function of pressure; the error bars are estimated from reasonable extrapolations of $\rho(T)$.

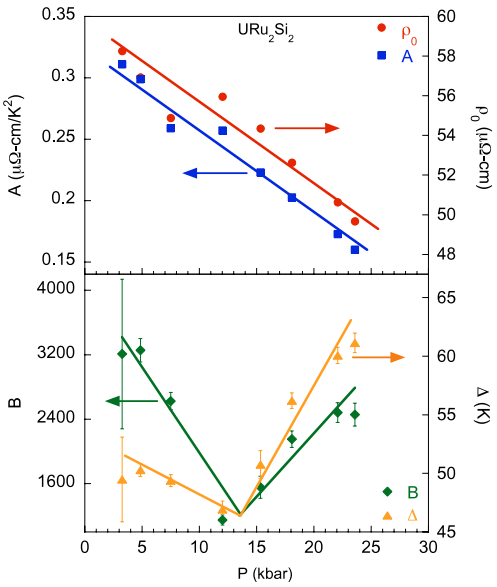

Figure 2. Fitting parameters from equation (1) as a function of pressure for the HO state of URu_2Si_2; the quantities are described in the text. (a) A (left axis) and ρ_0 (right axis). (b) B (left axis) and Δ (right axis). The solid lines are guides to the eye and error bars correspond to errors returned from the fitting algorithm.

the low-temperature value of the electrical resistivity at 2 K, $\rho(300\ \mathrm{K})/\rho(2\ \mathrm{K})$. With applied pressure, the room temperature value of the electrical resistivity changes very little, while the 2 K value of the electrical resistivity decreases by about 15%, leading to a RRR = 8.5 at the highest measured pressure of 23.6 kbar.

Figure 1 displays the electrical resistivity $\rho(T)$ as a function of temperature in the region of the HO/AFM transition for selected pressures P measured in this study. The distinctive peak and trough structure of the HO transition, with the transition temperature T_0 defined as the inflection point in the electrical resistivity, systematically increases in temperature with applied pressure. A change in the pressure dependence of T_0 is visible near 15 kbar, above which the feature associated with T_0 increases to higher temperatures more rapidly with little qualitative change in the shape of the feature (see T_0 versus P in figure 4). The width of the transition in temperature changes little with applied pressure; however, the height of the transition $\delta\rho$, defined by extrapolating the temperature dependence of the electrical resistivity above and below T_0 and evaluating the resultant change in $\rho(T)$ at T_0 (exemplified as the dashed lines for the $P = 4.9$ kbar data of figure 1), displays a moderate, yet significant, pressure dependence. The inset of figure 1 shows the pressure dependence of $\delta\rho$, the magnitude of which gradually decreases with pressure up to approximately 15 kbar, after which it remains roughly constant up to the maximum attained pressure. The interpretation of the pressure dependence of $\delta\rho$ will be discussed later.

The electrical resistivity below T_0 was fit with an expression involving a T^2 Fermi liquid term and an exponential term associated with magnetic order with a gap Δ in the magnon dispersion relation:

$$\rho(T) = \rho_0 + AT^2 + B\frac{T}{\Delta}\left(1 + \frac{T}{\Delta}\right)\mathrm{e}^{(-\Delta/T)}, \qquad (1)$$

with ρ_0, A, B, and Δ as fitting parameters, where ρ_0 is the residual resistivity, A is a measure of the quasiparticle effective mass, B is a measure of the spin-wave (magnon) stiffness, and Δ is the size of the gap in the magnon dispersion [16, 17, 39–42]. The use of this expression can be justified by the presence of commensurate and incommensurate gapped spin excitations as seen in previous and recent neutron scattering experiments [4, 43]. The parameters resulting from these fits at various pressures are shown in figure 2, with the error bars representing errors returned from the fitting algorithm and the solid lines being guides to the eye. The values for the fitting parameters are different than those reported for polycrystalline samples by McElfresh *et al* [16]; however, the general trends of the parameters with pressure are similar in this particular single crystal specimen. While ρ_0 and A evolve continuously, monotonically decreasing with pressure, the magnitudes of the gap Δ and B show a change in behavior in the vicinity of 15 kbar.

3.2. *Superconducting state*

A previously oriented and characterized sample (different from the one used in the hidden order state experiments described in section 3.1 above), with RRR = 10.6 and displaying a sharp superconducting transition at $T_c = 1.42$ K, was spark cut in half along the crystallographic a-axis (i.e., the freshly cut surface is perpendicular to the basal plane, nominally in an ac-plane). The two halves of the sample were mounted perpendicular to each other such that, when the high-pressure cell was mounted in the cryostat, the magnetic field was nominally aligned parallel to the c-axis for one sample and parallel to the a-axis (basal plane) for the other. In both

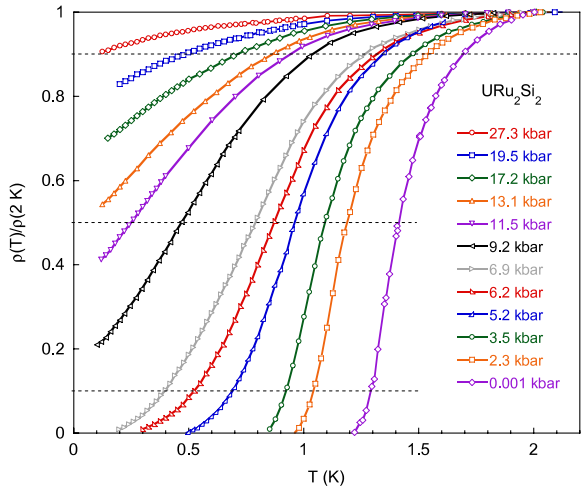

Figure 3. Low-temperature electrical resistivity normalized at 2 K, $\rho(T)/\rho(2\ \mathrm{K})$, versus T of URu_2Si_2 for various pressures showing the suppression of superconductivity. The horizontal dashed lines indicate, from top to bottom, the 90%, 50%, and 10% values of the resistive SC transition. T_c is defined as the temperature at which the resistive transition is 50% of its normal state value.

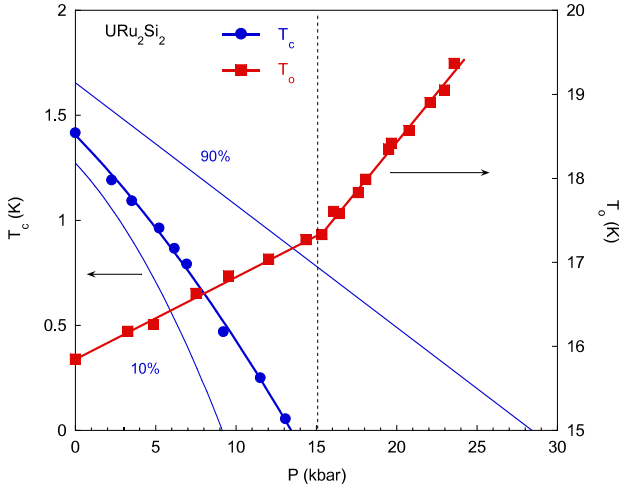

Figure 4. SC and HO $T-P$ phase diagram. The SC phase T_c (left axis) is demarcated by the blue filled circles (the line is a guide to the eye). The 90% and 10% values of the resistive transition from figure 3 are indicated as light blue lines (no symbols) forming an envelope around T_c. The HO/AFM phase (right axis) is indicated by the red squares with linear fits to the data above and below the critical pressure $P_c = 15$ kbar, which is represented by the vertical dashed line.

cases, the electrical current was applied in the basal plane and perpendicular to the applied field (i.e., $j \parallel a \perp H$). This permitted measurements of the upper critical field H_{c2} for two field orientations.

Figure 3 shows the zero-field electrical resistivity normalized to the normal state value at 2 K, $\rho(T)/\rho(2\ \mathrm{K})$, versus temperature T. The horizontal dashed lines indicate, from top to bottom, the 90%, 50%, and 10% values of the normalized electrical resistivity with the 50% value used to define the superconducting transition temperature T_c. The superconducting state is suppressed monotonically, as seen by the decrease in T_c, and the transition is slightly broadened with applied pressure. The superconducting transition develops a pronounced low-temperature tail at 5.2 kbar that widens with increasing pressure. For $P \geqslant 9.2$ kbar, a complete superconducting transition is not observed by 100 mK, the base temperature of our experimental setup; however, transitions to the 50% value of the normal state are evident up to 11.5 kbar, with a reasonable extrapolation of $T_c = 55$ mK at 13.1 kbar. Further increases in pressure results in a smooth evolution of the transition with the highest measured data at $P = 27.3$ kbar displaying a reduction in scattering down to 90% just above 100 mK.

4. Discussion

4.1. Zero-field phase diagram

Using the data in figures 1 and 3, a zero-field $T-P$ phase diagram of the HO/AFM and superconducting states has been generated as shown in figure 4. The HO transition temperature T_0 increases linearly with pressure up to 15 kbar, after which a distinct change in slope is seen and T_0 continues increasing with more than twice the slope of the low-pressure region. The red lines passing through the square symbols in figure 4 are linear fits to the data below and above 15 kbar yielding fits for the pressure dependence of T_0 with slopes equal to 0.10 and 0.23 K kbar^{-1}, respectively. The observed change in slope occurred at the pressure where the magnetic moment was previously shown to discontinuously increase to a value more consistent with bulk LMAFM [22]; this pressure is marked by the dashed vertical line on the figure at $P_c = 15$ kbar. The presence of a kink in the pressure dependence of T_0 is consistent with a SDW-based model for the HO state proposed by Mineev and Zhitomirsky [12]. Within this framework, the kink in T_0 implies that the order parameter of the HO state is decoupled from that of the LMAFM state, and furthermore suggests that the two forms of order are mutually exclusive and that the observed low-pressure moment arises from itinerant SDW-like order or extrinsic effects such as lattice strain. Furthermore, this scenario would dictate that the transition from the HO state to the LMAFM state is first-order in nature.

The superconducting critical temperature, defined as the 50% value of the normal state resistivity, decreases with increasing pressure, persisting up to nearly 14 kbar. This correspondence of the suppression of superconductivity near the position of the kink in the pressure dependence of T_0, itself related to the appearance of LMAFM and thus the destruction of hidden order, is in agreement with previously reported results [16, 23]. The pressure at which superconductivity is suppressed is, however, in contrast to results that indicate the destruction of superconductivity at relatively low pressures below 5 kbar [44]. Envelopes indicating the 10% and 90% values from figure 3 are plotted as light blue lines (no symbols) in figure 4, with the 10% envelope extending up to nearly 9 kbar, a pressure significantly higher than the 5 kbar critical pressure reported by Sato *et al* [44]. The 90% envelope exists well above P_c, extrapolating to zero at approximately

28.5 kbar. This could be a consequence of the inherently broad superconducting transition characteristic of URu_2Si_2 samples.

The results of this experiment would seem to implicate a critical pressure of $P_c = 15$ kbar, where T_c is suppressed and the pressure dependence of T_0 undergoes a change in slope, as the transition between the HO state and LMAFM; however, as the electrical resistivity is indirectly coupled through scattering processes to the order parameters of both states, a conclusive determination of the HO/AFM phase boundary cannot be advanced. There is, however, no evidence in the zero-field electrical resistivity measurements to support the supposition of a first-order phase transition between the HO and LMAFM phases occurring near 7 kbar. If, indeed, a first-order phase transition exists at this low pressure, as suggested by several other researchers [28–30], then the discontinuity in the order parameter is imperceptible by electrical resistivity measurements—implying that scattering is weakly affected by this putative phase boundary—and, additionally, the superconducting state is unaffected by the presence of such a phase boundary.

4.2. Critical fields

In addition to the zero-field measurements described in section 3.2, field-dependent measurements were performed at each pressure step including base temperature field sweeps and temperature sweeps at various fields. It should be noted that the zero-field value of T_c for the sample aligned with $H \parallel a$ is nearly 50 mk higher than that of the sample with $H \parallel c$. As these two samples were cut from the same larger specimen, the disparity in the zero-field T_c is likely due to slight inhomogeneity within the crystal or effects arising from the spark erosion process. The observed anisotropy in the field dependence of the superconducting state is so large, however, that the small difference in the zero-field value of T_c has little effect on the general behavior of URu_2Si_2 in field. Using the same criteria as described above to define T_c, a superconducting field temperature H–T phase diagram has been constructed for both field alignments $H \parallel c$ and $H \parallel a$. These phase diagrams are displayed in figure 5, where the solid lines are empirical fits to a parabolic function reminiscent of that proposed in the weak-coupling BCS theory for the thermodynamic critical field [45]:

$$H_{c2}(T) = H_{c2}(0)\left[1 - A\left(\frac{T}{T_c}\right)^2\right], \qquad (2)$$

where $H_{c2}(0)$ and A are fitting parameters, with the former being the upper critical field at zero temperature. Equation (2) provides a systematic determination of $H_{c2}(0)$ but provides few physical details or insights for the field dependence of the superconducting state, as would perhaps be garnered from fits involving digamma functions coupling the Pauli and orbital limits [46–48]. Perhaps surprisingly, the fitting parameter A obtained from these fits is in reasonable agreement with the BCS value of 1.07, with $A \approx 1.0$ and 0.9 for $H \parallel c$ and $H \parallel a$, respectively. The fact that equation (2) provides an acceptable empirical fit for all pressures in figure 5, and furthermore,

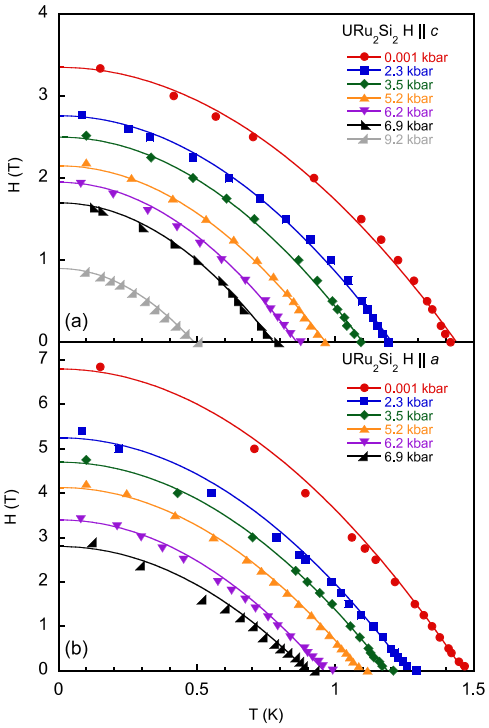

Figure 5. H–T critical field curves of URu_2Si_2 with $H \parallel c$ (a) $H \parallel a$ (b) for various pressures. The lines are fits to equation (2) used to determine the value of $H_{c2}(0)$.

results in similar values of A, suggests that the pairing mechanism responsible for superconductivity is unchanged with pressure. This fact further constrains the first-order transition line seen in neutron scattering and thermal expansion experiments [28–30] to be inconsequential to the formation and persistence of superconductivity. Slight disparities between the critical field data presented herein and those previously reported [23, 31], specifically the value of $H_{c2}(0)$, are likely due to small misalignments of the field with respect to the crystallographic axes of the samples.

Deviations from equation (2) can be seen near T_c, with the deviations being more pronounced for the sample with $H \parallel a$, where a positive curvature was revealed over a narrow temperature window below T_c. This curvature in the upper critical field line has been previously reported and attributed to anisotropic pairing in the presence of antiferromagnetic order [31]. No data exist for the $H \parallel a$ specimen above 6.9 kbar, because the sample fractured inside the pressure cell upon pressurization.

Using the values for $H_{c2}(0)$ and A determined from figure 5, the slopes of the upper critical field curves near T_c are obtained by evaluating the derivative of equation (2) at T_c. The slopes evaluated at T_c, $-\mathrm{d}H_{c2}(T)/\mathrm{d}T|_{T_c}$, are then used to estimate the orbital critical field at zero temperature $H^{\star}_{c2}(0)$ from the following weak-coupling formula [49]:

$$H^{\star}_{c2}(0) = 0.693 T_c \left(\frac{-\mathrm{d}H_{c2}(T)}{\mathrm{d}T}\right)\Big|_{T_c}. \qquad (3)$$

Estimates of the Pauli limited upper critical field, in units of tesla, are determined directly from T_c following Clogston [50]

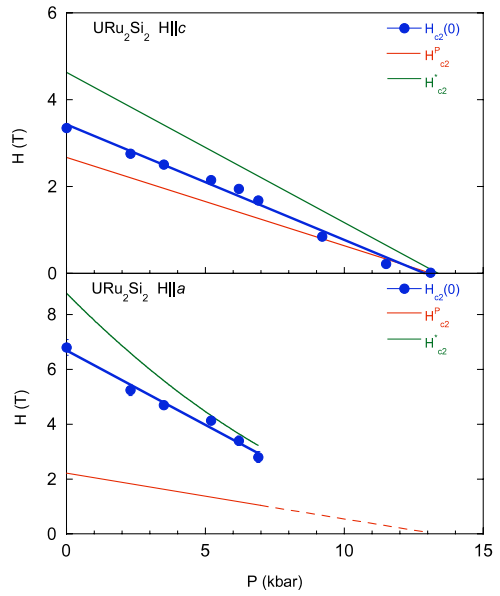

Figure 6. $H_{c2}(0)$ with $H \parallel c$ (a) and $H \parallel a$ (b) as a function of P with the calculated Pauli and orbitally limited critical fields displayed as red [below $H_{c2}(0)$] and green [above $H_{c2}(0)$] lines, respectively. The dashed portion of the line in (b) indicates that the Pauli limit is calculated from the zero-field T_c of the sample with $H \parallel c$.

and Chandrasekhar [51]:

$$H_{c2}^{p}(0) = 1.84 T_c, \tag{4}$$

where $H_{c2}^{p}(0)$ is the value of the Pauli limited upper critical field at zero temperature derived using BCS theory. Analysis of previous field-dependent specific heat measurements by Fisher *et al* [52]. indicate that $H_{c2}^{p}(0)$ determined from specific heat data via the condensation energy is in good agreement with the value expected from equation (4).

Figure 6 displays the values for the measured upper critical field, $H_{c2}(0)$, the estimated Pauli limited upper critical field, $H_{c2}^{p}(0)$, and the calculated zero temperature orbital critical field, $H_{c2}^{\star}(0)$, as function of pressure. For both field orientations, the measured upper critical field $H_{c2}(0)$ is enhanced above what would be expected for the Pauli limited case; however, while the value of $H_{c2}(0)$ for $H \parallel c$ is significantly lower than the orbital limit, the value of $H_{c2}(0)$ for $H \parallel a$ is very near the orbital limit.

The coherence length ξ_0 is calculated from the values of $H_{c2}^{\star}(0)$ obtained above using the formula:

$$\xi_0 = \sqrt{\frac{\Phi_0}{2\pi H_{c2}^{\star}(0)}},$$

where Φ_0 is the flux quantum. Using previously published values of the quasiparticle carrier density of approximately 0.05 carriers per U ion [53] and the Fermi velocity $v_F = 1.9 \times 10^6$ cm s^{-1} [54] along with the experimentally determined residual resistivity $\rho_0 \approx 25\ \mu\Omega$ cm, the quasiparticle mean free path l_{mfp} is estimated to be nearly 1100 Å, in good agreement with previous measurements [55, 56]. With ξ_0 of the order 100 Å, an order of magnitude less than l_{mfp}, it can be concluded, despite the small value of RRR, that URu_2Si_2 is in the clean limit; and, as such, many of the closed-form, analytical expressions describing the behavior of the superconducting state in the dirty limit are inapplicable.

4.3. Competing Fermi surfaces

It was proposed by Maple *et al* that the hidden order transition in URu_2Si_2 partially gapped the Fermi surface, with the remaining, ungapped portion of the Fermi surface undergoing superconductivity at low temperature [3]. In this scenario, the increase in T_0 corresponds to an increase in the amount of Fermi surface gapped by the hidden order state. As the amount of gapped Fermi surface increases, it reduces the number of electrons available to participate in superconducting pairing, thus lowering T_c as seen experimentally. The pressure-dependent resistivity measurements reported herein provide the means for both a qualitative and quantitative confirmation of this hypothesis. Using the theory developed by Bilbro and McMillan and later extended to SDW's by Machida, the competition between the hidden order and superconducting states of URu_2Si_2 can be expressed as [57, 58]:

$$T_{c0} = T_c(P)^{n(P)} T_0(P)^{1-n(P)}, \tag{5}$$

provided the coupling constants for the two ordered phases are comparable, where T_{c0} is the superconducting critical temperature in the absence of a high-temperature gap, T_c is the pressure-dependent value of the superconducting critical temperature, T_0 is the transition temperature of the HO/AFM transition, and n, a measure of the percentage of the Fermi surface that remains ungapped below T_0, is the ratio of the electronic specific heat coefficient above T_c to that of the normal state above T_0 (i.e., $n = \gamma_0/\gamma_{norm}$). Evaluating equation (5) at zero pressure and using $n = 0.58$ as determined from specific heat measurements by Maple *et al* [3] yields $T_{c0} = 3.9$ K. equation (5) can then be recast as:

$$n(P) = \frac{\ln\left(\frac{T_{c0}(P)}{T_0(P)}\right)}{\ln\left(\frac{T_c(P)}{T_0(P)}\right)} \tag{6}$$

and, using the transition temperatures T_c and T_0 from figure 4, used to calculate $n(P)$. The values obtained for $n(P)$ from this method are plotted in figure 7 as red circles, with the red line being a guide to the eye.

Plotted as green diamonds in figure 7, along with the values of $n(P)$ obtained above, are values of $n(P)$ estimated from experimental, pressure-dependent specific heat measurements performed by Fisher *et al* [52]. The previously reported electronic specific heat coefficients, determined from $C(T)/T$ just above T_c, have been normalized to a value of $\gamma_{norm} = 120.7$ mJ mol^{-1} K^{-2} such that $n(0) = 0.58$; an accurate estimate of the pressure dependence of γ_{norm} from [52] is difficult, but the previous data show little pressure dependence in γ_{norm}, justifying the normalization utilized above. The data from Fisher *et al* are in excellent agreement with the partially gapped Fermi surface results calculated from the superconducting and HO transition temperatures, suggesting that, regardless of the order parameter involved, a

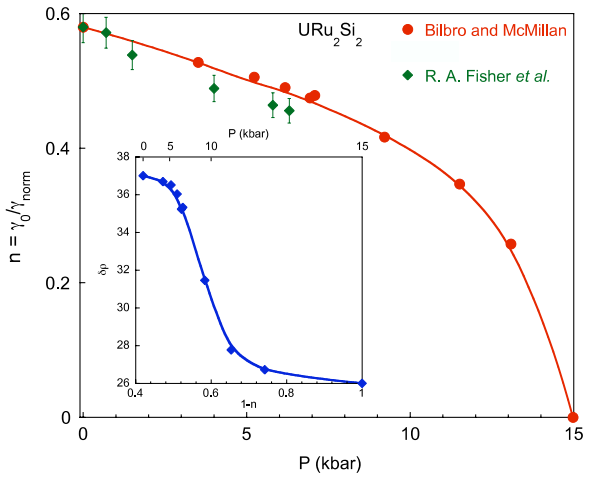

Figure 7. Fraction of the Fermi surface left ungapped by the HO/AFM transition, $n = \gamma_0/\gamma_{\rm norm}$, in URu_2Si_2 versus P. The red circles were calculated using the model of Bilbro and McMillan, while the green diamonds were estimated from data from Fisher *et al* [52], with error bars resulting from different estimates of the specific heat. The red line is a guide to the eye. Inset: $\delta\rho$ as a function of the fraction of Fermi surface gapped by the HO transition, $1 - n$, itself a non-linear function of pressure. The blue line is a guide to the eye.

partial gap at the Fermi surface develops below T_0 even under pressure. High pressure specific heat measurements in excess of 7 kbar are necessary to confirm this scenario.

The compound URu_2Si_2 has been shown to be a multiband, compensated metal [59–61]. The presence of metallic conduction at temperatures below T_0 precludes the HO transition from gapping the entire Fermi surface, which would result in a metal–insulator or superconducting transition at T_0. Instead, it is likely that the Fermi surface gap associated with HO occupies only a portion or pocket of the Fermi surface, thus providing residual density of states to permit metallic conduction below T_0. If a SDW-like picture is invoked to describe the HO state, then the partial gap induced by the onset of HO should be associated with nested pockets of the Fermi surface.

The apparent validity of this partially gapped Fermi surface picture would seem to suggest that the HO state fully gaps the portion of the Fermi surface on which it resides near 15 kbar. This description is consistent with the evolution of the height of the resistive signature at the HO transition $\delta\rho$. As pressure is applied to URu_2Si_2, the HO state gaps a larger fraction of its portion of the Fermi surface; as such, the number of available states into which quasiparticles may scatter is reduced, thus reducing the magnitude of the electrical resistivity. At and above the critical pressure of $P_c = 15$ kbar, the portion of the Fermi surface associated with HO is completely gapped, yielding a constant scattering term and a relatively pressure-independent value of $\delta\rho$ (see inset of figure 1). In the inset of figure 7, the value of $\delta\rho$ is shown as a function of $1 - n$, the fraction of the FS gapped by the HO/AFM transition, which is monotonic but non-linear in pressure. The non-linear behavior of $\delta\rho$ with $1 - n$ alludes to the complex pressure-dependent evolution of the scattering processes associated with the HO/AFM transition.

As the competing Fermi surface picture only requires the transition temperatures to calculate the pressure dependence, it is unable to distinguish between a scenario with phase segregated HO and LMAFM states, for which the volume fractions of both evolve with pressure, or a scenario with a HO-dominated state separated from a LMAFM-dominated state by a first-order transition. Furthermore, high-field de-Haas–van-Alphen measurements as a function of pressure reveal no change in Fermi surface structure [62]. Therefore, it is highly suggestive, from the reasonable agreement found with the application of the model of Bilbro and McMillan, that the HO and superconducting states must occupy the same portion or pocket of the Fermi surface.

5. Conclusions

We have investigated the effect of pressure on both the HO and superconducting phases of URu_2Si_2, with the field dependence of the latter examined at low temperatures. The HO transition temperature T_0 increases linearly with applied pressure at a rate of 0.10 K kbar^{-1} up to a critical pressure $P_c = 15$ kbar, after which the rate more than doubles to 0.23 K kbar^{-1}. This kink in the HO T–P phase diagram occurred at the same pressure at which LMAFM was seen to develop in neutron scattering experiments. The superconducting state persists nearly up to P_c, illustrating the coincidence of superconductivity and the HO state. Measurements of the upper critical field along both crystallographic directions reveal a strong anisotropy, where $H_{c2}(0)$ for $H \parallel a$ is dominated by spin–orbit effects resulting in upper critical fields significantly higher than those for $H \parallel c$. The upper critical field curves have been fit with an empirical parabolic expression that is valid across the pressure range measured, indicating that the underlying mechanism of superconductivity persists unchanged up to 9.2 kbar. The contrary evolution of the HO and superconducting transitions is explained via a partially gapped Fermi surface scenario in which the increase in the HO transition temperature corresponds to an increase in the portion of the Fermi surface that is gapped, thus reducing the number of states available for superconducting pairing. This scenario yields excellent quantitative agreement with previously reported specific heat results; and, furthermore, effectively describes the observed behavior of the magnitude of the HO transition $\delta\rho$. However, additional pressure-dependent specific heat measurements would be most helpful in verifying this proposal.

The destruction of superconductivity with the onset of LMAFM tends to suggest that the LMAFM phase does not favor the formation of superconducting pairs, meaning the superconductivity in URu_2Si_2 likely develops with the HO state, as suggested by the competition for Fermi surface fraction by the two ordered phases. The presence of the distinct kink in the T–P phase diagram of the HO/AFM state is consistent with the phenomenological description of URu_2Si_2 suggested by Mineev and Zhitomirsky [12]. Following this description, this kink implies that a first-order phase boundary exists between the HO and AFM states–which should be mutually exclusive, requiring the observed moment at low

pressures to be attributed to a SDW-like object or extrinsic effects—with $P_c = 15$ kbar serving as a critical pressure. The use of this model is further supported by the existence of both a gapped spin excitation spectrum, which suggested the form of equation (1), and a partial gap at the Fermi surface,which promoted the aforementioned application of the partially gapped Fermi surface model.

The simultaneous presence of gapped spin excitations and a partial Fermi surface gap conspires to suggest that a SDW-like Fermi surface instability occurs at T_0. If such an instability is indeed responsible for the HO transition, then the charge and spin gaps should be related, as they arise from the same fundamental mechanism within the framework of a conventional, mean-field description of an SDW where the details are dictated by the coupling strength and the magnitude of an itinerant SDW moment [63]. The lack of any observed metal–insulator transition, which should accompany the formation of a SDW in a simple material, is consistent with URu_2Si_2 being a more complicated multiband, compensated metal [59–61], which would permit metallic conduction with multiple scattering mechanisms below a SDW-like transition. As the measurements presented herein do not couple to the staggered magnetization or the order parameter of the HO state, the details of any HO/AFM first-order transition cannot be directly probed.

Acknowledgments

The authors wish to thank J Paglione for many useful discussions. Crystal synthesis was sponsored by the U.S. Department of Energy (DOE) under Research Grant # DE-FG02-04ER46178. High-pressure research presented herein was supported by the National Nuclear Security Administration under the auspices of the Stewardship Stockpile Academic Alliances program through DOE Research Grant # DE-FG52-06NA26205. Lawrence Livermore National Laboratory is operated by Lawrence Livermore National Security, LLC, for the U.S. Department of Energy, National Nuclear Security Administration under Contract DE-AC52-07NA27344.

References

[1] Palstra T T M, Menovsky A A, van den Berg J, Dirkmaat A J, Kes P H, Nieuwenhuys G J and Mydosh J A 1985 *Phys. Rev. Lett.* **55** 2727
[2] Schlabitz W, Baumann J, Pollit B, Rauchschwalbe U, Mayer H M, Ahlheim U and Bredl C D 1986 *Z. Phys.* B **62** 171
[3] Maple M B, Chen J, Dalichaouch Y, Kohara T, Rossel C, Torikachvili M S, McElfresh M W and Thompson J D 1986 *Phys. Rev. Lett.* **56** 185
[4] Broholm C, Kjems J K, Buyers W J L, Matthews P, Palstra T T M, Menovsky A A and Mydosh J A 1987 *Phys. Rev. Lett.* **58** 1467
[5] Chandra P, Coleman P, Mydosh J A and Tripathi V 2002 *Nature* **417** 1831
[6] Santini P and Amoretti G 1994 *Phys. Rev. Lett.* **73** 1027
[7] Fazekas P, Kiss A and Radnóczi K 2005 *Preprint* cond-mat/0506504
[8] Kiss A and Fazekas P 2005 *Phys. Rev.* B **71** 054415
[9] Okuno Y and Miyake K 1998 *J. Phys. Soc. Japan* **67** 2469
[10] Agterberg D F and Walker M B 1994 *Phys. Rev.* B **50** 563
[11] Ikeda H and Ohashi Y 1998 *Phys. Rev. Lett.* **81** 3723
[12] Mineev V P and Zhitomirsky M E 2005 *Phys. Rev.* B **72** 014432
[13] Barzykin V and Gor'kov L P 1993 *Phys. Rev. Lett.* **70** 2479
[14] Varma C and Zhu L 2006 *Phys. Rev. Lett.* **96** 036405
[15] Fawcett E 1988 *Rev. Mod. Phys.* **60** 209
[16] McElfresh M W, Thompson J D, Willis J O, Maple M B, Kohara T and Torikachvili M S 1987 *Phys. Rev.* B **35** 43
[17] Palstra T T M, Menovsky A A and Mydosh J A 1986 *Phys. Rev.* B **33** 6527
[18] Bonn D A, Garrett J D and Timusk T 1988 *Phys. Rev. Lett.* **61** 1305
[19] Park J-G, McEwen K A, deBrion S, Chouteau G, Amitsuka H and Sakakibara T 1997 *J. Phys.: Condens. Matter* **9** 3065
[20] Sharma P A, Harrison N, Jaime M, Oh Y S, Kim K H, Batista C D, Amitsuka H and Mydosh J A 2006 *Phys. Rev. Lett.* **97** 156401
[21] Pfleiderer C, Mydosh J A and Vojta M 2006 *Phys. Rev.* B **74** 104412
[22] Amitsuka H, Sato M, Metoki N, Yokoyama M, Kuwahara K, Sakakibara T, Morimoto H, Kawarazaki S, Miyako Y and Mydosh J A 1999 *Phys. Rev. Lett.* **83** 5114
[23] Brison J P *et al* 1994 *Physica* B **199–200** 70
[24] Amitsuka H, Tenya K, Yokoyama M, Schenck A, Andreica D, Gygax F N, Amato A, Miyako Y, Huang Y K and Mydosh J A 2003 *Physica* B **326** 418
[25] Matsuda K, Kohori Y, Kohara T, Kuwahara K and Amitsuka H 2001 *Phys. Rev. Lett.* **87** 087203
[26] Matsuda K, Kohori Y, Kohara T, Amitsuka H, Kuwahara K and Matsumoto T 2003 *J. Phys.: Condens. Matter* **15** 2363
[27] Shah N, Chandra P, Coleman P and Mydosh J A 2000 *Phys. Rev.* B **61** 564
[28] Bourdarot F *et al* 2005 *Physica* B **359–361** 986
[29] Knebel G, Izawa K, Bourdarot F, Hassinger E, Salce B, Aoki D and Flouquet J 2007 *J. Magn. Magn. Mater.* **310** 195
[30] Motoyama G, Nishioka T and Sato N 2003 *Phys. Rev. Lett.* **90** 166402
[31] Kwok W K, DeLong L E, Crabtree G W, Hinks D G and Joynt R 1990 *Phys. Rev.* B **41** 11649
[32] Bakker K, deVisser A, Bruck E, Menovsky A A and Franse J J M 1992 *J. Magn. Magn. Mater.* **108** 63
[33] Guillaume A, Salce B, Flouquet J and Lejay P 1999 *Physica* B **259–261** 652
[34] Mason T, Gaulin B, Garrett J D, Tun Z, Buyers W J L and Isaacs E D 1990 *Phys. Rev. Lett.* **65** 3189
[35] Smith T F, Chu C W and Maple M B 1969 *Cryogenics* **9** 53
[36] Varga T, Wilkinson A P and Angel R J 2003 *Rev. Sci. Instrum.* **74** 4564
[37] Sidorov V A and Sadykov R A 2005 *J. Phys.: Condens. Matter* **17** S3005
[38] Jayaraman A, Hutson A R, McFee J H, Coriell A S and Maines R G 1967 *Rev. Sci. Instrum.* **38** 44
[39] Andersen N H and Smith H 1979 *Phys. Rev.* B **19** 384
[40] Andersen N H 1980 *Crystalline Electric Field and Structural Effects in f-electron Systems* ed J E Crow, R P Guertin and T W Mihalisin (New York: Plenum) p 373
[41] Larrea J, Fontes J M M, Alvarenga A D, Baggio-Saitovitch E M, Burghardt T, Eichler A and Continentino M A 2005 *Phys. Rev.* B **72** 035129
[42] Mentink S A M, Mason T E, Süllow S, Nieuwenhuys G J, Menovsky A A, Mydosh J A and Perenboom J A A J 1996 *Phys. Rev.* B **53** R6014
[43] Wiebe C R *et al* 2007 *Nat. Phys.* **3** 96
[44] Sato N, Uemura S, Motoyama G and Nishioka T 2006 *Physica* B **378–380** 576
[45] Bardeen J, Cooper L N and Schrieffer J R 1957 *Phys. Rev.* **108** 1175

[46] Helfand E and Werthamer N R 1966 *Phys. Rev.* **147** 288
[47] Werthamer N R, Helfand E and Hohenberg P C 1966 *Phys. Rev.* **147** 295
[48] Maki K 1966 *Phys. Rev.* **148** 370
[49] Hake R R 1967 *Appl. Phys. Lett.* **10** 189
[50] Clogston A M 1962 *Phys. Rev. Lett.* **9** 266
[51] Chandrasekhar B 1962 *Appl. Phys. Lett.* **1** 7
[52] Fisher R A, Kim S, Wu Y, Phillips N E, McElfresh M W, Torikachvili M S and Maple M B 1990 *Physica* B **163** 419
[53] Behnia K *et al* 2005 *Phys. Rev. Lett.* **94** 156405
[54] Ohkuni H, Ishida T, Inada Y, Haga Y, Yamamoto E, Onuki Y and Takahashi S 1997 *J. Phys. Soc. Japan* **66** 945
[55] Ohkuni H *et al* 1999 *Phil. Mag.* B **79** 1045
[56] Brison J P, Keller N, Verniere A, Lejay P, Schmidt L, Buzdin A, Flouquet J, Julian S R and Lonzarich G G 1995 *Physica* C **250** 128
[57] Bilbro G and McMillan W L 1976 *Phys. Rev.* B **14** 1887
[58] Machida K 1981 *J. Phys. Soc. Japan* **50** 2195;
Machida K and Matsubara T 1981 *J. Phys. Soc. Japan* **50** 3231;
Machida K 1982 *J. Phys. Soc. Japan* **51** 1420;
Machida K 1983 *J. Phys. Soc. Japan* **52** 1333
[59] Inada Y and Onuki Y 1999 *Low Temp. Phys.* **25** 573
[60] Ito T, Kumigashira H, Takahashi T, Haga Y, Yamamoto E, Honma T, Ohkuni H and Onuki Y 1999 *Phys. Rev.* B **60** 13390
[61] Denlinger J D, Gweon G H, Allen J W, Olson C G, Maple M B, Sarrao J L, Armstrong P E, Fisk Z and Yamagami H 2001 *J. Electron Spectrosc. Relat. Phenom.* **117** 347
[62] Nakashima M, Ohkuni H, Inada Y, Settai R, Haga Y, Yamamoto E and Onuki Y 2003 *J. Phys.: Condens. Matter* **15** S2011
[63] Grüner G 1994 *Rev. Mod. Phys.* **66** 1